Sea Grant Colleg[illegible] Program

Massachusetts Institute
of Technology
Cambridge, Massachusetts
02139

CABLE DYNAMICS FOR TETHERED UNDERWATER VEHICLES

Michael S. Triantafyllou
Franz Hover

MITSG90-4

Sea Grant College Program
Massachusetts Institute of Technology
Cambridge, MA 02139

Grant No: NA86AA-D-SG089
Project No: RU-21

Table of Contents

List of Figures

Cable Dynamics for Tethered Underwater Vehicles

1 Abstract

The dynamics of tethered underwater vehicles are affected significantly by the presence of the tether, particularly in deep water when the mass and drag of the cable are comparable, or even much larger than the drag and inertia of the vehicle itself.

A numerical scheme is provided herein to study the dynamics of tethered vehicles, which exploits a variety of previous findings in cable dynamics to simplify the governing equations without affecting noticeably the accuracy of the solution. Woods Hole Oceanographic Institution's vehicles, such as ARGO and JASON, are used as example cases and full scale results confirm the validity of the numerical predictions.

2 Introduction

Tethered underwater vehicles find a wide range of applications. Some are positioned through controlling the surface support ship, because they make a very reliable and economic means for continuous ocean exploration. Others carry their own thrusters, but use the umbilical cable for power and communication transmission.

In all cases, however, the tether introduces significant dynamic phenomena, because it carries substantial inertial and fluid drag loads. Hence, in order to properly understand and possibly improve the dynamics of the underwater vehicle, one must have an accurate model of the cable at hand.

A cable presents unusual difficulties as a dynamical system, because it is a mechanism, rather than a simple structural member, i.e. it accomodates external loads through substantial shape changes. As a result, the cable configuration is an unknown itself, rendering a simulation by necessity nonlinear and quite complex. Also, when a cable moves in water it is subject to large fluid forces, the principal of which is separation drag, a force which is notoriously difficult to model because it is accompanied by vortex formation and an assortment of complex fluid phenomena, while its functional dependence, even within the simple Morison formulation, is nonlinear, thus adding to the complexity of the problem. In fact, one may state safely that **knowledge of cable dynamics in air is entirely useless when studying**

problems in water, because of the dramatic changes caused by nonlinear drag.

Cable dynamics have attracted considerable attention for a variety of applications, while the theoretical interest is also considerable (see Irvine 1981, Triantafyllou 1983 and Triantafyllou 1987a). Several authors have addressed problems similar to the one at hand, i.e. the behaviour of a cable used to tow a body. In the references we have provided a number of citations for work on the field, including recent contributions.

A substantial effort has been expended over the last ten years in the Design Laboratory at M.I.T. studying the dynamics of cables. As a result, we are in the position to develop models which are computationally efficient, while they contain all essential physical mechanisms of cable response. The present report outlines in some detail the application of such models and the associated numerical codes to surface-controlled vehicles. Full scale data are used to corroborate the findings.

3 Previous Work

4 Analytical Model Derivation

The cable and vehicle models described here have their origin in Triantafyllou (1986, 1987b) and Hover (1989). In the cable model the unwieldy finite-difference equations are avoided in favour of a Galerkin spectral method employing a finite Fourier series, resulting in far fewer computational elements. The vehicle motions present a fairly standard problem in rigid-body dynamics, and they provide the boundary conditions for the lower end of the cable; the upper end motions are taken to be exactly those of the ship (the motions of the ship are assumed to be unaffected by the cable and vehicle dynamics). One major simplifying feature of the model is that it solves the dynamics around a predefined static configuration, created by a current profile and/or steady tow speed condition.

5 Equations of Motion and Statics

Newton's Law applied to a differential element of the cable provides the equations of motion for the cable. We first note that if the unstretched length of an element is ds, then the stretched length dp is related to ds by the following equation:

$$\frac{dp}{ds} = 1 + \varepsilon \tag{1}$$

where ε is the strain in the element. Letting m be the mass per unit stretched length, **v** the absolute velocity vector of the element, **R** the applied force per unit stretched length, and **F** the internal force, Newton's Law gives (see Figure 1):

$$\frac{d}{dt}(m\,\mathbf{v}\,dp) = d\mathbf{F} + \mathbf{R}\,dp \tag{2}$$

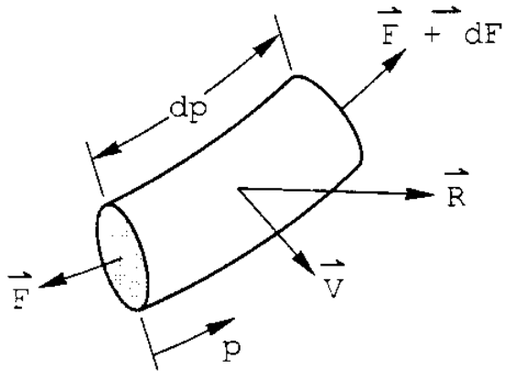

Figure 1: Free Body Diagram for Cable Element

Employing mass conservation, we are left with the following equation:

$$m\frac{d\mathbf{v}}{dt} = \frac{d\mathbf{F}}{dp} + \mathbf{R} \tag{3}$$

Several simplifications can be made at this stage. First, the bending rigidity is assumed to be negligible; for a cable under high tension (relative to the total magnitude of the distributed loads, such as drag and weight forces), the moments associated with the curvature alone are much higher than the internal moments due to bending stresses. The effects of torsional moments can be neglected also, since the eigenvalue problem for torsional dynamics shows the first modes to be exceptionally fast relative to both the maneuvering and wave-induced frequencies. Also the tension in the cable is assumed to be quasi-static; i.e., there are no elastic travelling waves. Again, the reason is that the eigenvalue problem for the elastic response gives very high frequency modes.

We choose to solve the problem in cable coordinates, and select the cable frame to coincide with the *material* tangential, normal, and binormal vectors. The rotation vector ω is used to account for time

variance of the reference frame, while the Darboux vector Ω is used to account for the spatial changes in the reference frame. For an arbitrary vector **f** in the cable frame, total derivatives can be expressed as:

$$\frac{d\mathbf{f}}{dt} = \frac{\partial \mathbf{f}}{\partial t} + \omega \times \mathbf{f} \tag{4}$$

$$\frac{d\mathbf{f}}{ds} = \frac{\partial \mathbf{f}}{\partial s} + \Omega \times \mathbf{f} \tag{5}$$

Three Euler Angles are normally used to transform quantities between inertial and cable reference frames - it is convenient to express both the rotation and Darboux vectors in terms of these angles.

In general, **R** consists of gravity and drag forces, while **F** is simply $(T\,\mathbf{t})$, where **t** is the tangent vector, and T is the tension scalar. Accounting for stretching in the static configuration, we find:

$$0 = \frac{d(T\,\mathbf{t})}{dp} + \mathbf{R} \tag{6}$$

or

$$0 = \frac{\partial T}{\partial p}\,\mathbf{t} + T\frac{d\mathbf{t}}{dp} + \mathbf{R} \tag{7}$$

Only the in-plane motions will be considered here, which are taken to be uncoupled from the out-of-plane motions. In this special case, $\frac{d\mathbf{t}}{dp}$ is the spatial rate of change of the cable's inclination angle ϕ, and Frenet's relations from Hildebrand (1976) show that this derivative is in the normal direction. We eventually arrive at the following two equations which completely describe the static configuration in the tangential and normal directions:

$$0 = w\,sin(\phi) - \frac{dT}{dp} + \frac{1}{2}\rho\,C_f\,d\,U\cos(\phi)\,|U\cos(\phi)| \tag{8}$$

$$0 = w\,cos(\phi) - T\frac{d\phi}{dp} - \frac{1}{2}\rho\,C_d\,d\,U\sin(\phi)\,|U\sin(\phi)| \tag{9}$$

where w is the cable weight in water per stretched unit length, d is the cable diameter, C_d is the drag coefficient, C_f is the frictional coefficient, and the velocity U is provided by an arbitrary horizontal current field. Elongation of the cable is due to tension (Hooke's Law) and to hydrostatic pressure; both of these quantities typically change with depth. See the description of the hydrostatic pressure effect in Appendix

1. Cable diameter d is reduced from these elongations, through Poisson's Ratio. Finally, we should note that when the cable is nearly vertical, the tangential drag is negligible.

The initial conditions, in terms of the values of ϕ and T at the bottom of the cable, are found by setting the aggregate forces and moments on the vehicle equal to zero--this also provides the static inclination angle of the vehicle. In the sequel, the static cable angle is termed ϕ_s.

6 Compatibility Relations

The dynamics as well as the statics are derived from (3) . The strategy will be to solve for the dynamics as deflections from the static configuration, which can be found beforehand. For this, we need to identify the geometric compatibility relations.

Compatibility can be expressed in terms of positions or velocities. The velocity-based results have the advantage that they are independent of the reference system, but in this work we have used the position-based relations. To begin, let the '0' subscript denote quantities in the static sense; deflections from these static configurations will be studied. In Figure 2, if $\mathbf{r}_0$ is the static position vector, and $\mathbf{r}$ is the dynamic position vector, then the deflection $\underline{\mathbf{r}}$ is defined as:

$$\underline{\mathbf{r}} = \mathbf{r} - \mathbf{r}_0 \tag{10}$$

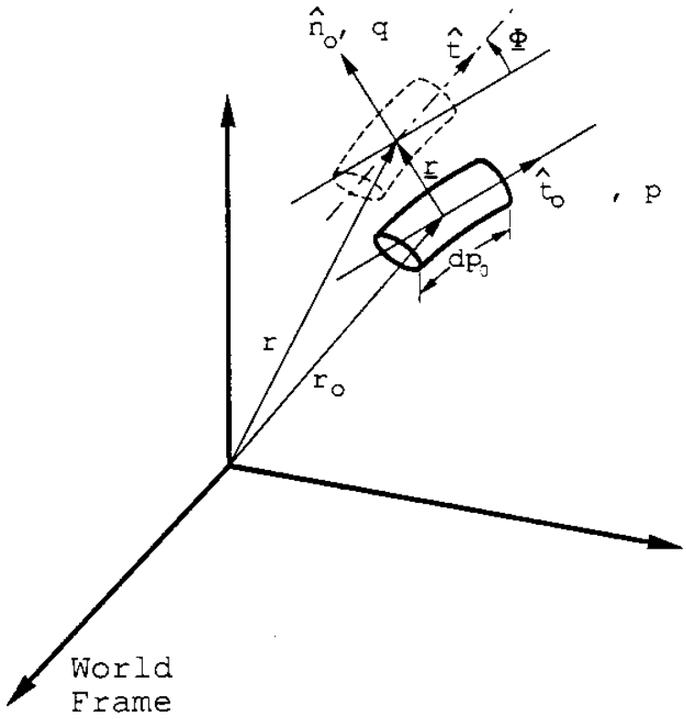

Figure 2: Geometric Compatibility

Letting Ω_0 be the Darboux vector expressed in the static cable coordinate frame, we find that

$$\frac{d\mathbf{r}}{dp_0} - \frac{d\mathbf{r}_0}{dp_0} = \frac{\partial(\mathbf{r} - \mathbf{r}_0)}{\partial p_0} + \Omega_0 \mathbf{x} (\mathbf{r} - \mathbf{r}_0) \tag{11}$$

Now, let

$$\mathbf{t} = \frac{d\mathbf{r}}{dp} \tag{12}$$

and

$$\mathbf{t}_0 = \frac{d\mathbf{r}_0}{dp_0} \tag{13}$$

Combining terms into (11), we get

$$(1 + \varepsilon)\mathbf{t} - (1 + \varepsilon_0)\mathbf{t}_0 = \frac{\partial(\mathbf{r} - \mathbf{r}_0)}{\partial s} + \Omega_0 \mathbf{x} (\mathbf{r} - \mathbf{r}_0)(1 + \varepsilon_0) \tag{14}$$

For reference, the velocity relations are easily found by differentiating this relation with respect to time. For the two-dimensional, position-based analysis, $\underline{r}$ is projected onto the static cable reference system $<\mathbf{t}_0,\mathbf{n}_0>$. Letting p be the axial deflection and q be the lateral deflection, $\underline{r}$ is written as

$$\underline{r} = \mathbf{t}_0 p + \mathbf{n}_0 q \tag{15}$$

and the dynamic tangent vector is expressed in terms of the angular deflection (ϕ, in the static cable reference frame:

$$\mathbf{t} = \mathbf{t}_0 \cos(\phi) + \mathbf{n}_0 \sin(\phi) \tag{16}$$

For the two-dimensional case,

$$\Omega_0 = \frac{\partial \phi_s}{\partial p_0} \mathbf{b}_0 \tag{17}$$

Making a small-angle assumption for ϕ, the final result turns out to be:

$$\varepsilon_d = \frac{\partial p}{\partial s} - q \frac{\partial \phi_s}{\partial s} \tag{18}$$

$$\phi_d (1 + \varepsilon_0) = \frac{\partial q}{\partial s} + p \frac{\partial \phi_s}{\partial s} \tag{19}$$

Each of these results is now incorporated in the equations of motion that were outlined above. First, (18) integrated over the length of the cable yields the dynamic elongation of the cable, taking into account the effects of static curvature. Namely,

$$\Delta L = p_L - p_0 - \int_0^L \frac{\partial \phi_s}{\partial s} q \, ds \tag{20}$$

Along with the constitutive law, this gives the dynamic tension in the cable due to elongation and transverse deflections. It follows from the static equation (8), subject to our simplification of the axial dynamics, that

$$T_d = \frac{EA}{L} \left[p_L - p_0 - \int_0^L \frac{\partial \phi_s}{\partial s} q \, ds \right] - F_{dt} p \tag{21}$$

where F_{dt} is the dynamic external force in the tangential direction, which acts in addition to the force found for the static configuration.

Concerning the second compatibility relation (19), it is assumed that the dynamic angle due to axial motion of the cable is small with respect to the angle induced by dynamic lateral motions. This is motivated by, and substantiated through consideration of the physical system: the vertical motions are small compared to the length. Coupling the dynamic and static terms in Newton's form, we have, after some algebra,

$$m \frac{\partial^2 q}{\partial^2 t} = (T_s + T_d) \frac{\partial^2 q}{\partial^2 p} + T_d \frac{\partial \phi_s}{\partial p} + F_{dn} \tag{22}$$

Here, the pure static component from the coupling multiplication falls out, having been solved in the static case. Physically, the second term on the right side represents the cable's ability to straighten under a dynamic tension. Again, F_n is the external force in the normal direction.

7 Solving the Modified Wave Equation

The problem is greatly facilitated by non-dimensionalization. First, let $\alpha = \frac{\partial \phi_s}{\partial s}$, and let T_r be some representative tension in the cable(e.g., at the midpoint). The following definitions are made:

$$\omega_n = \frac{\pi}{L}\sqrt{T_r / m}$$

$$\tau = t\,\omega_n$$

$$x = \frac{s}{L}$$

$$\eta = \frac{q}{d}$$

$$\xi = \frac{p}{d} \tag{23}$$

$$\alpha_0 = \frac{\alpha}{L}$$

$$H_s = \frac{T_s}{T_r}$$

$$H_d = \frac{T_d}{T_r}$$

Noting a slight change in derivative notation, i.e. we denote the derivative of a dependent variable u with respect to a variable z by u_z, we begin with the dimensional form of the wave equation (22):

$$m\,q_{tt} = (T_d + T_s)\,q_{ss} + T_d\,\alpha - F_{dn} \tag{24}$$

and using the new non-dimensional variables, obtain

$$\eta_{\tau\tau} = \frac{T_r (H_d + H_s)}{m L^2 \omega_n^2}\eta_{xx} + \frac{T_r H_d \alpha_o L}{m d \omega_n^2} - \frac{F_{dn}}{m d \omega_n^2} \tag{25}$$

F_{dn} will be defined as the external normal force per unit length in the negative-q direction:

$$F_{dn} = \frac{1}{2}\rho_w C_d d\,|V_r|\,V_r \tag{26}$$

where V_r is composed of the combination of absolute incident flow, and the imposed flow due to the

cable's own motion. About the equilibrium point, this normal force is

$$F_{dn} = \frac{1}{2} C_d d \rho_w (|q_t - \underline{U}| (q_t - \underline{U}) - |-\underline{U}|(-\underline{U})) \tag{27}$$

with $\underline{U} = U \sin(\phi_s)$. Non-dimensionalization and substitution into (25) gives:

$$\eta_{\tau\tau} = \frac{T (H_d + H_s)}{m L^2 \omega_n^2} \eta_{xx} + \frac{T H_d \alpha_o}{m d \omega_n^2 L} - \frac{1}{2} D Z \tag{28}$$

The simplified terms D and Z are given as follows:

$$D = \frac{\rho d^2}{m} \tag{29}$$

$$Z = C_d (|\eta_\tau - \frac{\underline{U}}{\omega_n d}| (\eta_\tau - \frac{\underline{U}}{\omega_n d}) + \frac{\underline{U}^2}{d^2 \omega_n^2}) \tag{30}$$

Making further use of the nondimensional terms, (28) becomes:

$$\eta_{\tau\tau} = \frac{(H_s + H_d)}{\pi^2} \eta_{xx} + \frac{H_d \alpha_o L}{\pi^2 d} - \frac{1}{2} D Z \tag{31}$$

The solution to this partial differential equation is expanded using the Fourier theorem into an infinite sum of sinusoids plus additional terms to accomodate the boundary conditions, i. e.,

$$\eta(x,t) = \eta_1(1 - x) + \eta_2 x + \sum_{n=1}^{\infty} Q_n \sin(n\pi x) \tag{32}$$

The construction of a dynamic cable configuration is shown in Figure 3; a) shows the static catenary in a steady tow state, and b), c), and d) superimpose the first two, four, and eight harmonics, respectively. Often apparently complex cable shapes are described adequately with a small number of sinusoids.

The nondimensional dynamic tension on the cable is expressed as (from (23)):

$$H_d = \frac{E A d}{T_r L} (\xi_2 - \xi_2 - \int_0^L \alpha_o \eta \, ds) + \frac{F_{dn} s}{T_r} \tag{33}$$

where

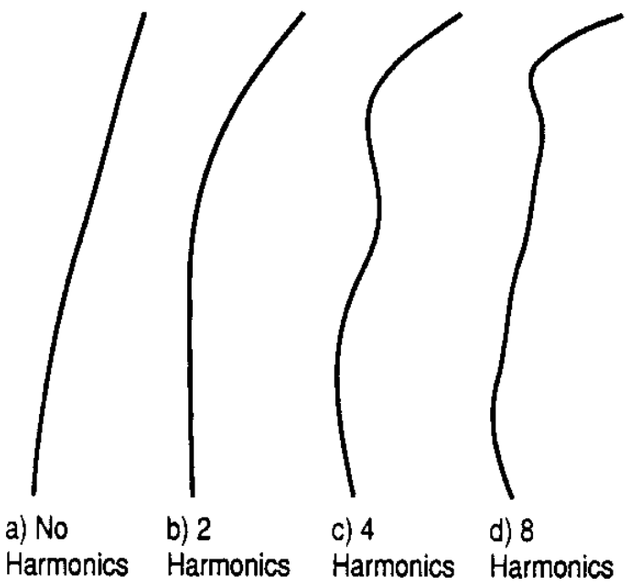

Figure 3: Harmonic Cable Configuration Dynamics

$$F_{dt} = \frac{1}{2}\rho_w C_f |V_t| V_t d \tag{34}$$

In this case, it is assumed that $\cos(\phi_s)$ is small enough that tangential drag effects due to the flow field in the fixed frame can be neglected, when compared to those generated by the cable motion alone. Then V_t is the velocity of the cable itself, which can be averaged along the cable as

$$V_t = \frac{p_{2t} - p_{1t}}{2}$$

or

$$V_t = \frac{1}{2} d\, \omega_n (\xi_{\tau 2} + \xi_{\tau 1}) \tag{35}$$

Some algebraic manipulation gives a new form for (33):

$$H_d = \frac{E\,A\,d}{T_r L}(\xi_2 - \xi_1 - \int_0^1 \alpha_o\,\eta\,dx) + \frac{\rho\,C_f\,d^3\,\omega_n{}^2\,L\,x}{8\,T_r}|\xi_{\tau 2} + \xi_{\tau 1}|(\xi_{\tau 2} + \xi_{\tau 1}) \tag{36}$$

We will find more utility in a simpler form for the dimensionless dynamic tension, namely,

$$H_d = H_d{}^o + \delta H_d\,\Xi \tag{37}$$

where the definitions are made:

$$H_d{}^o = \frac{E\,A\,d}{T_r L}(\xi_2 - \xi_1 - \int_0^1 \alpha_o\,\eta\,dx) \tag{38}$$

$$\delta H_d = \frac{\rho\,C_f\,d^3\,\omega_n{}^2\,L}{8\,T_r} \tag{39}$$

$$\Xi = |\xi_{\tau 2} + \xi_{\tau 1}|(\xi_{\tau 2} + \xi_{\tau 1}) \tag{40}$$

Insertion of the solution from (32) into the expression for $H_d{}^o$ yields

$$H_d{}^o = \frac{E\,A\,d}{T_r L}(\xi_2 - \xi_1 - \int_0^1 \alpha_o\,(\eta_1(1-x) + \eta_2 x + \sum_{n=1}^{ns} Q_n\,sin(n\,\pi\,x))\,dx) \tag{41}$$

This is

$$H_d{}^o = \frac{E\,A\,d}{T_r L}(\xi_2 - \xi_1 - \eta_1\,(I_2 - I_1) - \eta_2\,I_1 - \sum_{n=1}^{ns} Q_n\,I_3{}^n) \tag{42}$$

where the integrals I are defined as follows:

$$I_1 = \int_0^1 \alpha_o\,x\,dx$$

$$I_2 = \int_0^1 \alpha_o\,dx \tag{43}$$

$$I_3{}^n = \int_0^1 \alpha_o \, sin(n\pi x) \, dx$$

We let the static tension be comprised of a primary part and a spatially-varying part: $H_s = 1 + \delta H_s$. This leaves the wave equation (31) in the following form:

$$\eta_{\tau\tau} = \frac{1}{\pi^2}(1 + \delta H_s + H_d{}^o + \delta H_d \, x \, \Xi)\, \eta_{xx} + \frac{L}{\pi^2 d} H_d \, \alpha_o - \frac{1}{2} D \, Z \tag{44}$$

and insertion of the assumed solution (32) in its expanded form gives

$$\eta_{1\tau\tau}(1 - x) + \eta_{2\tau\tau} x + \sum_{n=1}^{ns} Q_{n\tau\tau} sin(n\pi x) = \tag{45}$$

$$\frac{1 + \delta H_s + H_d{}^o + \delta H_d \, x \, \Xi}{\pi^2} \sum_{n=1}^{ns} Q_n (n\,\pi)^2 \, (-sin(n\pi x)) +$$

$$\frac{L}{\pi^2 d}(H_d{}^o + \delta H_d \, x \, \mathrm{N})\, \alpha_o - \frac{1}{2} D \, Z$$

The equations are subsequently Galerkin-projected along the components of the Fourier expansions; i.e., each term is multiplied by sin(mπx), for m an integer, and integrated over the length. Making use of the identities

$$\int_0^1 x \, sin(n\,\pi\, x)\, dx = \frac{-(-1)^n}{n\,\pi} \tag{46}$$

$$\int_0^1 sin(n\,\pi\, x)\, dx = \frac{1 - (-1)^n}{n\,\pi}$$

and of orthogonality, lengthy algebraic manipulation eventually gives

$$Q_{m\tau\tau} + m^2 Q_m = \frac{2}{m\,\pi}(-\eta_{1\tau\tau} + \eta_{2\tau\tau}(-1)^m) -$$

$$2 \sum_{n=1}^{ns} Q_n \, n^2 \int_0^1 \delta H_s \, sin(n\,\pi\, x)\, sin(m\,\pi\, x)\, dx -$$

$$2 \sum_{n=1}^{ns} Q_n \, n^2 \, H_d{}^o \int_0^1 sin(n\,\pi\, x)\, sin(m\,\pi\, x)\, dx - \tag{47}$$

$$2 \sum_{n=1}^{ns} Q_n n^2 \delta H_d N \int_0^1 \sin(n \pi x) \sin(m \pi x) x \, dx +$$

$$\frac{2 L H_d^o}{\pi^2 d} \int_0^1 \alpha_o \sin(m \pi x) \, dx +$$

$$\frac{2 L \delta H_d N}{\pi^2 d} \int_0^1 x \alpha_o \sin(m \pi x) \, dx -$$

$$D \int_0^1 Z \sin(m \pi x) \, dx$$

For simplification, we define

$$I_4^{nm} = -2 n^2 \int_0^1 \delta H_s \sin(n\pi x) \sin(m\pi x) \, dx$$

$$I_5^{nm} = -2 n^2 \delta H_d \int_0^1 x \sin(n\pi x) \sin(m\pi x) \, dx \tag{48}$$

$$I_6^m = \frac{2 L}{\pi^2 d} \int_0^1 \alpha_o \sin(m \pi x) \, dx$$

$$I_7^m = \frac{2 L \delta H_d}{\pi^2 d} \int_0^1 x \alpha_o \sin(m \pi x) \, dx$$

providing the equations in the form:

$$Q_{m\tau\tau} + m^2 Q_m = \frac{2}{m \pi} (-\eta_{1\tau\tau} + \eta_{2\tau\tau}(-1)^m) + \sum_{n=1}^{ns} Q_n I_4^{nm} -$$

$$Q_m m^2 H_d^o + \Xi \sum_{n=1}^{ns} Q_n I_5^{nm} + I_6^m H_d^o + \Xi I_7^m - \tag{49}$$

$$D \int_0^1 Z \sin(m \pi x) \, dx$$

Also we note that

$$\int_0^1 x \sin(n \pi x) \sin(m \pi x) \, dx = -2 n m \frac{1 - (-1)^{n+m}}{(n^2 - m^2)^2} \text{ if } n \neq m \tag{50}$$

$$\int_0^1 x \sin(n \pi x) \sin(m \pi x)\, dx = \frac{1}{4} \text{ if } n = m$$

The final cable equations are contained in (49); each component presents a nonlinear ordinary differential equation, coupled to the rest. It should be noted that for a cable with two-dimensional configuration, to first order there is no coupling between in-plane (tangential and normal) and out-of-plane motions (binormal), except for fluid forces. If all three motions must be considered, the out of plane motion can be described, within the same approximation, by the same equation as the transverse in-plane motion, except that the static curvature effects must be ommitted. This will approximate the solution in three dimensions. When both in-plane and out-of-plane motions are being modelled, care must be taken to see that the drag forces reflect the vector nature of the overall drag effect (hence providing coupling of the in-plane and out-of-plane motions). One should also note that for a cable in air there are nonlinear geometric terms coupling the in-plane and out-of-plane motions, which must be included for accurate solution of the equations. Such coupling terms in water, however, are overwhelmed by the drag nonlinearity and can be ommitted, except for very low frequencies.

The vehicle dynamics must be next addressed to establish the response of the lower endpoint.

8 Vehicle Dynamics

This section addresses the full three-dimensional dynamic vehicle response. The Morison formulation is used to account for drag and inertial forces.

Newton's Law in translation and rotation gives:

$$m\frac{d\mathbf{v}}{dt} = \mathbf{F}_{added\,mass} + \mathbf{F}_{buoy} + \mathbf{F}_{wt} + \mathbf{F}_{tension} + \mathbf{F}_{drag} \tag{51}$$

$$\mathbf{I}_v\frac{d\boldsymbol{\omega}}{dt} = \mathbf{M}_{addedmass} + \mathbf{M}_{buoy} + \mathbf{M}_{wt} + \mathbf{M}_{tension} + \mathbf{M}_{drag} \tag{52}$$

It is simplest to express the components of the velocity vector **v** and the rotation vector ω in the vehicle reference frame - for this reason, the Euler Angle rotations are again convenient. We define a matrix $\mathbf{C}_v$ which maps vector coordinates expressed in an inertial frame into the vehicle frame, through three Euler Angles. Further, $\mathbf{C}_c$ is a matrix which transforms coordinates from the inertial frame to the cable reference frame, at the lower end of the cable.

The temporal change of the velocity and rotational velocity, as viewed from the vehicle frame, can be found after expressing the total derivatives through the rotation vector. We find that:

$$\frac{\partial\mathbf{v}}{\partial t} = (m\,\mathbf{I} + \mathbf{A}_m)^{-1}(\mathbf{F}_{buoy} + \mathbf{F}_{wt} + \mathbf{F}_{tension} + \mathbf{F}_{drag} - m\,\boldsymbol{\omega}\times\mathbf{v}) \tag{53}$$

$$\frac{\partial\boldsymbol{\omega}}{\partial t} = \mathbf{I}_v^{-1}(\mathbf{M}_{buoyancy} + \mathbf{M}_{weight} + \mathbf{M}_{tension} + \mathbf{M}_{drag} - \mathbf{r}_{am}\times\mathbf{A}_m\frac{\partial\mathbf{v}}{\partial t} - (\mathbf{I}_v\,\boldsymbol{\omega})\times\boldsymbol{\omega}) \tag{54}$$

Here, **I** is the identity matrix, $\mathbf{A}_m$ is the added mass matrix, and $\mathbf{r}_{am}$ is the vector which locates the added mass center (defined in analogy to the mass center) on the body.

The various forces are specified in the vehicle frame with the use of the transformation matrices $\mathbf{C}_c$ and $\mathbf{C}_v$:

$$\mathbf{F}_{buoyancy} = B\,\mathbf{C}_v\,\mathbf{z} \tag{55}$$

$$\mathbf{F}_{weight} = -W\,\mathbf{C}_v\,\mathbf{z} \tag{56}$$

$$\mathbf{F}_{tension} = T\,\mathbf{C}_v\,\mathbf{C}_c^{-1}\,\mathbf{t} \tag{57}$$

$$\mathbf{F}_{drag} = -\frac{1}{2}\rho_w C_d\,\mathbf{v}\,(\mathbf{v}\cdot\mathbf{A}) \tag{58}$$

where $\dot{\mathbf{z}}$ is the unit vector in the inertial vertical direction, and **A** is the vehicle area vector, i.e. a vector whose coordinates are equal to the projected vehicle area in the corresponding direction. The corresponding moments are the cross products of these forces with their respective location vectors.

The absolute velocity is simply the inverse-transformed body-referenced velocity vector:

$$\frac{\partial \mathbf{x}}{\partial t} = \mathbf{C}_v^{-1}\,\mathbf{v} \tag{59}$$

The time rate of change of the Euler Angles is a little more difficult to obtain. First, the rotation vector in the absolute frame is equal to the vectorial sum of the Euler Angle rates, each going through only some part of the whole transformation. Given the order of the rotations, it is possible through substitution to extract the individual Euler Angle rates, as a function of the current angles and the rotation vector; see Appendix **2**. This transformation matrix we call **S**, and we get:

$$\frac{\partial \Theta}{\partial t} = \mathbf{S}\,\omega \tag{60}$$

where Θ is the vector of Euler Angles. It now remains only to transform the motions of the vehicle's cable connection point back into cable coordinates so that the cable problem can be propagated. The total motions can be considered as the summed effects of rotations of the vehicle and translation of its center, and we use the transformation matrices $\mathbf{C}_c$ and $\mathbf{C}_v$ as before to move between reference systems. The following results are in the cable frame at the bottom of the cable:

$$\mathbf{x}_c = \mathbf{C}_c\,(\mathbf{C}_v^{-1}\,\mathbf{r}_c + \mathbf{x}) \tag{61}$$

$$\frac{d\mathbf{x}_c}{dt} = \mathbf{C}_c\,\mathbf{C}_v^{-1}\,(\mathbf{v} + \omega \times \mathbf{r}_c) \tag{62}$$

$$\frac{d^2\mathbf{x}_c}{dt^2} = \mathbf{C}_c\,\mathbf{C}_v^{-1}\,(\frac{\partial \mathbf{v}}{\partial t} + \frac{d\omega}{dt} \times \mathbf{r}_c + \omega \times (\omega \times \mathbf{r}_c) + 2\,\omega \times \mathbf{v}) \tag{63}$$

Here, $\mathbf{r}_c$ is the cable connection point location vector. These relations provide the lower-end quantities required for (49). For the top end of the cable, excitation motions need to be transformed into cable coordinates, similarly to what was done for the vehicle end.

9 Implementation Notes

9.1 Statics

Before any of the dynamics can be addressed, it is necessary to determine the steady-state configuration of the system, in the presence of a flow field due to the forward velocity and/or the current profile. Equations (51) and (52), after ommiting dynamic terms, are the basis for finding the vehicle's orientation. The vehicle inclination and the cable angle at the point of attachment are the unknowns, and it is a simple matter of recursively solving the equations (51) and (52) for these twounknowns. Following this, the cable angle and tension are integrated up to the surface using (8) and (9). Quantities which need to be saved during the space integration include the local tension, flow field, and curvature.

9.2 Solving the Dynamics

The resulting equations of Section 7 are actually solvable by any ordinary differential equation integrator. The two-dimensional problem was originally solved using Newmark's Method with a corrector loop, which is well suited to second-order nonlinear systems. However, if vehicle motions are to be followed in three dimensions, the differential equations in velocity are separable from those in position, and we have chosen the standard Runge-Kutta algorithm for propagation of all the first-order equations. Although the dynamics in surge for a long cable are known to be very slow, the expression for the dynamic tension itself may turn out to be very stiff: as a result, the integration time step must typically be much smaller than the horizontal response alone would dictate.

Obviously, for increasing resolution along the cable, and for increasing numbers of harmonics, the accuracy of the analytical model improves. In general, however, good results have been obtained with about thirty cable sections, and not many more than ten sinusoids. Certain responses, such as the step response, may require higher resolution in both respects, due to the importance of properly simulating the inherent delay in propagation of transverse disturbances along the cable. In addition, a longer length and/or lighter vehicle require a larger number of sinusoidal components. It should be noted that an effect akin to aliasing can occur if the number of spectral components is too great compared to the number of cable segments; this will lead to incorrect, if not outright unstable, system responses.

10 Application to the ARGO/JASON Vehicles

The physical system is shown in figure 4: A surface ship positions, usually at slow speed, an underwater vehicle through a long tether. The vehicle may be searching the ocean floor, or mapping the topography of the bottom, or it may be the platform for a smaller vehicle equipped with its own thrusters.

The tether has length at least slightly larger than the water depth. Since the average depth of the ocean is about 4,000 m, with about 85% of the ocean being deeper than 2,500 m, tethers are usually very long, having very slow dynamics with time constants in the range of 1 to 5 min.

A series of experiments reported in Yoerger et al (1988), Triantafyllou et al (1988) and Grosenbaugh et al (1989) established the basic properties of the vehicle and cable systems. The data were collected in the Navy's AUTEC range in the Bahamas (1987), and in open sea experiments in the Tyrrhenian sea (1988).

Figure 5 shows the response of the vehicle (dotted line) to a specific imposed ship motion (solid line) measured in the AUTEC range. The light dotted line shows the simulated vehicle response employing the numerical codes described here. The vehicle used here was a simple sphere with mass 2,200 kg and weight in water 18,800 N, while the cable was 1,200 m long, with diameter 1.72 cm, Young's modulus 6.2 10^{10} N/m^2 and specific density 4.4. Agreement between simulated and measured response is consistently good, with the cable drag coefficient being the single most important parameter (in this run the value of c_D was taken to be 1.6).

Figure 6 shows the simulated response of the MANGUS vehicle to the same surface excitation for three different cable lenths, 740 m; 1200 m; and 2,500 m, demonstrating the substantial reduction in vehicle bandwidth as the cable length increases.

Figure 7 shows the simulated response of the MANGUS vehicle to a 0.5 m/sec step velocity change of the surface vehicle and for three cable lengths 500 m; 1,000 m; 2,500 m, demonstrating the associated pure time delay estimated at 7 sec; 12 sec; 27 sec, respectively, for the three lengths considered.

Verification of the theoretical and numerical developments has concentrated on low frequency motions for lack of higher frequency data. It is hoped that full scale experiments planned for the Fall 1989 will provide the missing data. It should be noted that in fact the methodology outlined here is best-suited for higher frequency motions.

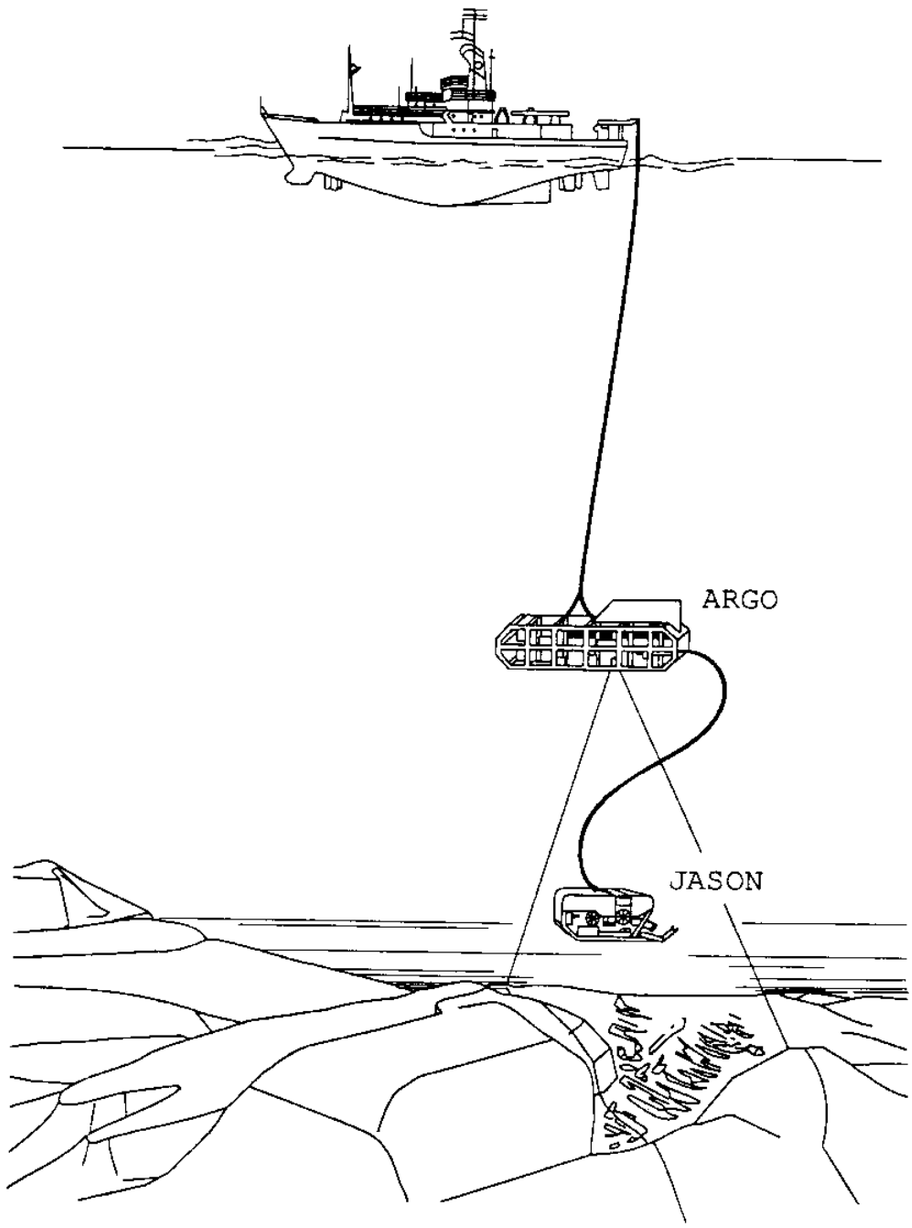

Figure 4: Towed Vehicle Configuration

We provide a case of higher frequency excitation as predicted by numerical simulation. It is for the vehicle ARGO, which has weight in air 20,000 N and buoyancy 10,000 N, in 1,500 m of water with the surface ship moving forward at 1 knot while undergoing heave oscillations of frequency 0.8 rad/sec and

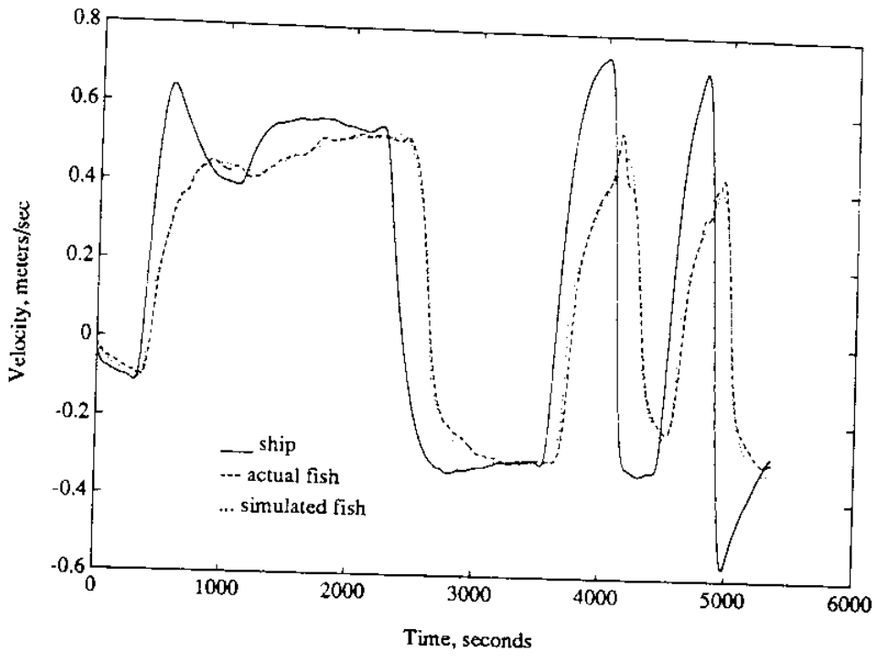

Figure 5: Vehicle Response

amplitude 1 m. As shown in figure 8, representing 40 sec of simulation time, the motion in a vertical plane containing the ship direction is not sinusoidal: The upward motion is much faster than the downward motion since in the latter case the vehicle is allowed to "fly" under lower tension. A basic feature of this simulation is the magnitude of response of the vehicle in the heave direction: it is almost completely undamped. This should serve as a warning to system designers that, unlike transverse motions, motions imposed along the axis of the cable (as is the heave motion in the case of this nearly vertical cable) are transmitted with very little damping all the way to the vehicle, however long the cable may be.

In fact, if the first axial natural frequency of the system is excited (i.e. the natural frequency obtained if we view the vehicle as a mass and the cable as a spring with mass), then the motions of the vehicle may be amplified, relative to the imposed motions of the ship. This in turn may cause momentary loss of tension in the line and subsequent snapping (high tension built-up) leading possibly to failure. Because of the importance of this subject and the special remedies it may require (heave compensation) we have

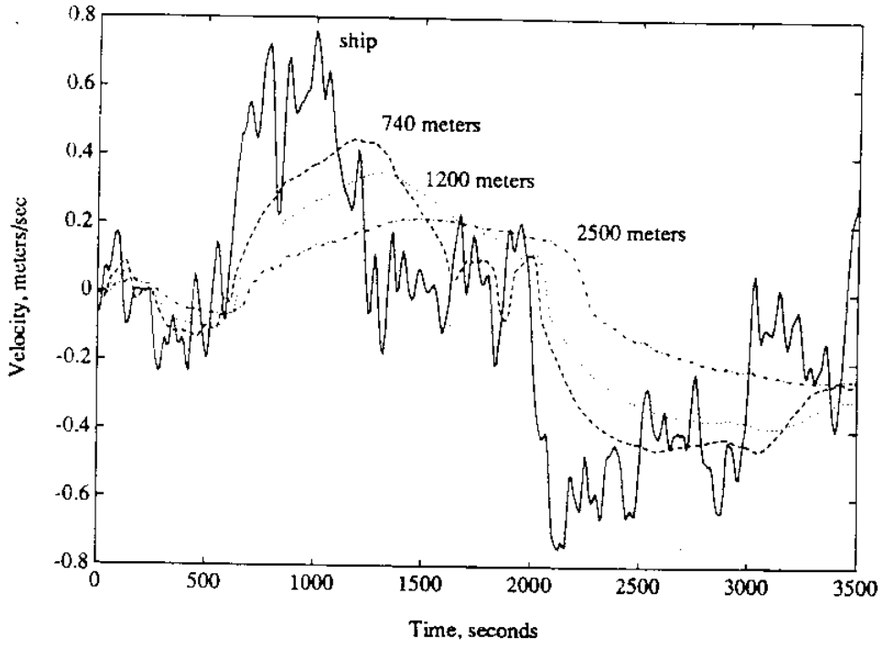

Figure 6: Vehicle Response

planned some experiments in the near future (1989) to address these issues.

11 Conclusions

A methodology has been presented to simulate efficiently the dynamics of a towed underwater vehicle. The equations as presented here are for two-dimensional motion, they are easily extendable, however, to the three-dimensional case. We plan to report this extension, together with the necessary verification in a future report.

The basic advantage of the present scheme is the ease of implementation; and the speed of running the code with good accuracy, as comparison with full scale experiments demonstrates.

It is hoped that the present methodology will lead to improved system designs, while further work is underway to enhance the capability of the developments reported here.

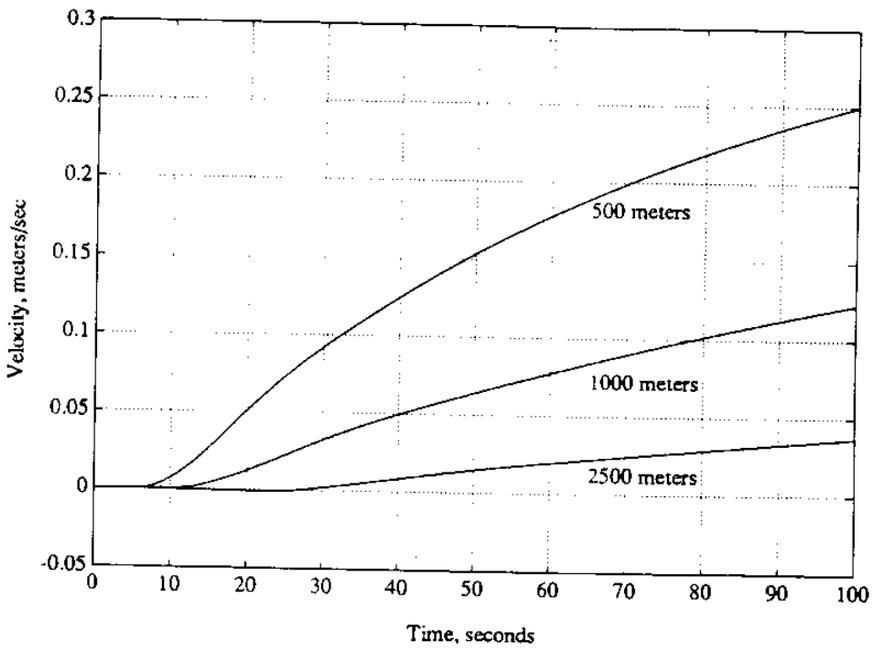

Figure 7: Vehicle Response

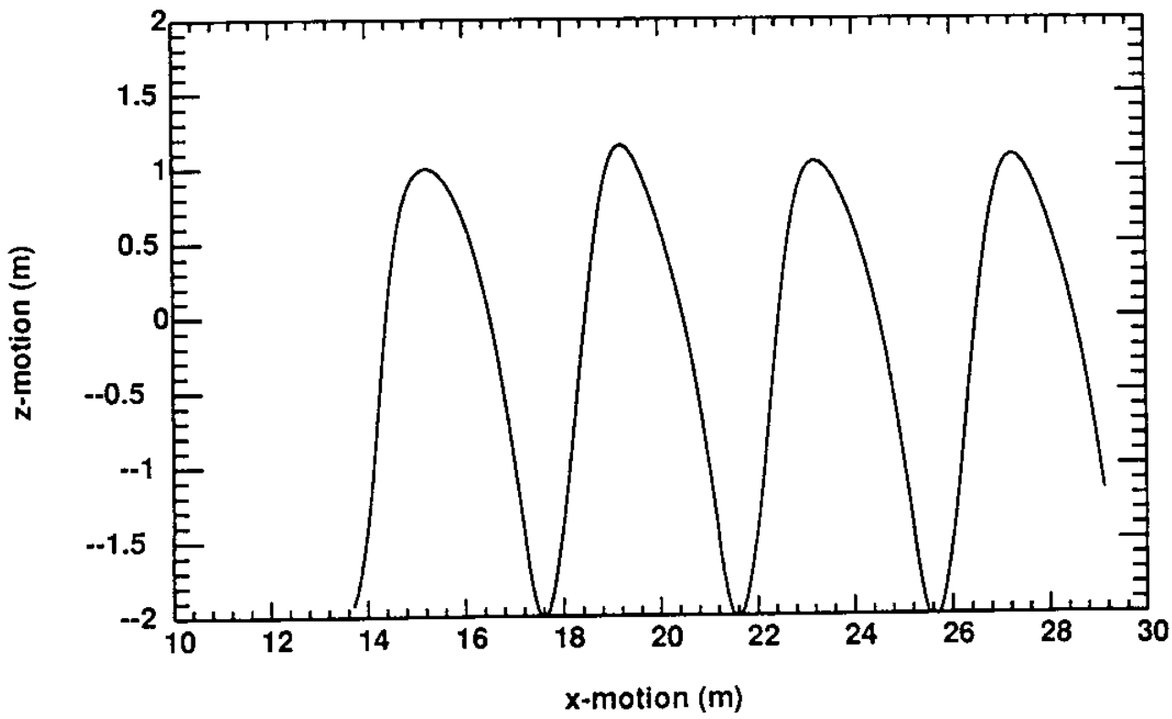

Figure 8: ARGO Response

12 REFERENCES

1. J. M. Abel, 1972, "Cable Interactions in a Depth Controlled Submersible", *Journal of Hydronautics*, Vol. **6**, No. 2, pp. 83-89.

2. C. M. Ablow and S. Schechter, 1983, "Numerical Simulation of Undersea Cable Dynamics", *Ocean Engineering*, Vol. **10**, pp. 443-457.

3. R. W. Bettles and D. A. Chapman, 1985, "Experimental Verification of a Towed Body and Cable Dynamics Response Theory", *Ocean Engineering*, Vol. **12**, No. 5, pp. 435-469.

4. T. C. Cannon and J. Genin, 1972, "Dynamical Behaviour of Marerially Damped Flexible Towed Cable", *Aeronautical Quarterly*, Vol. **23**, Pt. 2, pp. 109-120.

5. T. C. Cannon and J. Genin, 1972, "Three-Dimensional Dynamical Behaviour of a Flexible Towline", *Aeronautical Quarterly*, Vol. **23**, Pt. 3, pp. 201-210.

6. Y. I. Choo and M. J. Casarella, 1971, "Hydrodynamic Resistance of Towed Cables", *Journal of Hydronautics*, Vol. **5**, pp. 126-131.

7. Y. I. Choo and M. J. Casarella, 1973, "A Survey of Analytical Methods for Dynamic Simulation of Cable-Body Systems", *Journal of Hydronautics*, Vol. **7**, pp. 137-144.

8. Y. Cohen and H. Manor, 1988, "Equilibrium Configurations of a Cable Drogue System Towed in Helical Motion", *International Journal of Engineering Science*, Vol. 26, No. **8**, pp. 771-786.

9. T. N. Delmer, T. C. Stephens, 1989, "Numerical Simulation of an Oscillating Towed Weight", *Ocean Engineering*, Vol. **16**, No. 2, pp. 143-172.

10. A. P. Dowling, 1988, "The Dynamics of Towed Flexible Cylinders. Part 1 : Neutrally Buoyant Cylinders. Part 2: Negatively Buoyant Cylinders", *Journal of Fluid Mechanics*, Vol. **187**, pp. 507-571.

11. M. S. Firebaugh, 1972, "An Analysis of the Dynamics of Towing Cables", *PhD Thesis*, Massachusetts Institute of Technology, Cambridge, MA.

12. J. Genin and T. C. Cannon, 1967, "Equilibrium configuration and Tension of a Flexible Cable in Uniform Flowfield", *AIAA Journal of Aircraft*, Vol. **4**, p. 200.

13. J. Genin, S. J. Citron and R. R. Huffman, 1972, "Coupling of Longitudinal and Transverse Motions of a Flexible Cable in a Uniform Flow Field", *Journal of the Acoustical Society of America*, Vol. **52**, N0. 1, Pt. 2, pp. 438-440.

14. Goodman T. R. and Breslin J. P., 1976, "Statics and Dynamics of Anchoring Cables in Waves", *Journal of Hydronautics*, Vol. **10**, No. 4, pp. 113-120.

15. M. A. Grosenbaugh, D. R. Yoerger and M. S. Triantafyllou, 1989, "[illegible]-Scale Experimental Study of the Effect of Shear Current on the Vortex-Induced [illegible]on and Quasi-Static Configuration of a Long Tow Cable", *ASME Proc. of the Eighth Intern. Conference on Offshore Mech. and Arctic Engineering Symposium*, The Hague, The Netherlands.

16. F. B. Hildebrand, 1976, "Advanced Calculus for Applications", Second Ed., *Prentice-Hall, Inc.*: Englewood Cliffs, New Jersey

17. Hover F., 1989, "Deeply-Towed Underwater Vehicle Systems: A Verified Analytical Procedure for Creating Parametrized Dynamic Models", *S.M. Thesis*, Department of Mechanical Engineering, Massachusetts Institute of Technology, Cambridge, Mass.

18. R.R. Huffman and J. Genin, 1971, "The Dynamical Behaviour of a Flexible Cable in Uniform Flow Field", *Aeronautical Quarterly*, Vol. **22**, Pt. 2, pp. 183-195

19. Irvine H. M., 1981, "Cable Structures", *MIT Press*: Cambridge, Mass.

20. N. E. Jeffrey, 1968, "Influence of Design Features on Underwater Towed System Stability", *Journal of Hydronautics*, Vol. **2**, No. 4., pp. 205-213

21. J. Ketchman and Y. K. Lou, 1975, "Application of the Finite Element Method to Towed Cable Dynamics", *Proceedings OCEANS '75*, San Diego, CA.

22. J. W. Leonard, 1979, "Newton-Raphson Iterative Method Applied to Circularly Towed Cable-Body System", *Engin. Structures*, Vol. **1**, pp. 73-80.

23. J. W. Leonard and J. H. Nath, 1981, "Comparison of Finite Element and Lumped Parameter Methods for Oceanic Cables", *Engin. Structures*, Vol. **3**, pp. 153-167.

24. B. Paul and A. I. Soler, 1972, "Cable Dynamics and Optimum Towing Strategies for Submersibles", *Marine Technology Society Journal*, Vol. **6**, No. 2, pp. 34-42.

25. W. H. Phillips, 1949, Theoretical Analysis of a Towed Cable", *Technical Note* TN 1796, NACA.

26. L. Pode, 1951, "Tables for Computing the Equilibrium Configuration of a Flexible Cable in a Uniform Stream", *Report* 687 (AD607448),David Taylor Model Basin, Washington, DC.

27. S. P. Reyle and J. W. Schram, 1968, "Analysis of Three-Dimensional Towed System", *Unpublished Report*, Rutgers University, New Brunswick, NJ.

28. J.V. Sanders, 1982, "A Three-Dimensional Dynamic Analysis of a Towed System", *Ocean Engineering*, Vol. **9**, No. 5, pp. 483-489.

29. L. Schneider, L. G. Burton and T. Mahan, 1965, "Tow Cable Snap Loads", *Marine Technology*, Vol. **1**, pp. 42-49.

30. A. Simpson and B. Tabarrok, 1976, "On the Equilibrium Configuration of a Chain Subjected to Uniform Fluid Flow in a Horizontal Plane", *International Journal of Mech. Sci.*, Vol. **18**, pp. 91-94.

31. C. E. Smith and J. H. Nath, 1972, "Parameters Affecting the Natural Frequencies of Buoy/Taut Line Systems", *Marine Technology Society Journal*, Vol. **6**, No. 3, pp. 49-50.

32. Triantafyllou M. S., 1983, "Linear Dynamics of Cables and Chains", *The Shock and Vibration Digest*, Vol. **16**, No. 3, pp. 9-17.

33. M. S. Triantafyllou, A. Bliek, J. Burgess, and H. Shin, 1986, "Mooring Dynamics for Offshore Applications, Part 1", *Sea Grant College Program Report*, MIT, Cambridge, Massachusetts',

34. Triantafyllou M. S., 1987a, "Dynamics of Cables and Chains", *The Shock and Vibration Digest*, Vol. **19**, No. 12, pp. 3-5.

35. M. S. Triantafyllou, 1987b, "Notes for Cable Dynamics", *Unpublished Report*, Massachusetts Institute of Technology, Cambridge, Mass.

36. Triantafyllou M.S., Engebretsen K., Burgess J.J., Yoerger D.R., Grosenbaugh M.A., 1988, "A Full-Scale Experiment and Theoretical Study of the Dynamics of Underwater Vehicles Employing Very Long Tethers", *Proceedings Behaviour of Offshore Structures* (BOSS '88), Trondheim, Norway.

37. Yoerger D.R., Grosenbaugh M.A., Triantafyllou M.S., Engebretsen K., Burgess, J.J., 1988, "An Experimental Analysis of the Quasi-Statics and Dynamics of a Long Vertical Tow Cable", *ASME Proceedings of the Seventh International Conference on Offshore Mechanics and Arctic Engineering* , Houston, Texas.

38. N. Yoshikawa and T. Yabuta, 1983, "Study on Submarine Cable Tension During Laying", *IEEE Journal of Oceanic Engineering*, Vol. **OE-8**, No. 4, pp. 293-299.

13 Appendix

13.1 Effective Tension

A cable section under high ambient pressure experiences an elongation due to the pressure, in addition to the stretching induced by pulling on the ends. The basis of this extra elongation is seen in Figure 9, where Archimedes' view of the cable element is appended with a tensile pressure effect to result in the actual physical state of the cable element. The contribution of this added pressure component is:

$$T_{eff} = T_{pulling} + p\,A$$

where p is the ambient pressure, and A is the cross-sectional area of the cable. In our work, the **effective tension** (Goodman and Breslin 1976) is most applicable when the static cable configuration is under study; large dynamic motions are required to significantly change the hydrostatic pressure.

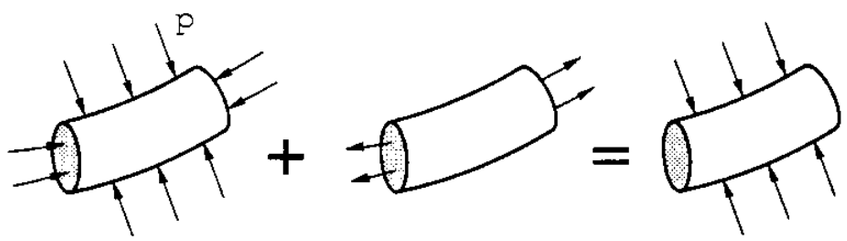

Figure 9: Effective Tension

13.2 Propagating the Euler Angles

This section describes how the matrix **S** can be found, given the order of rotation.

For this example, we let the rotations from the inertial frame occur in the following order:

1. Rotation about the (inertial-frame) z-axis (z) by θ
2. Rotation about the new y-axis (y_1) by ϕ
3. Rotation about the final new x-axis (x_2) by ψ

and the vehicle axes are $<x_3, y_3, z_3>$. See Figure 10.

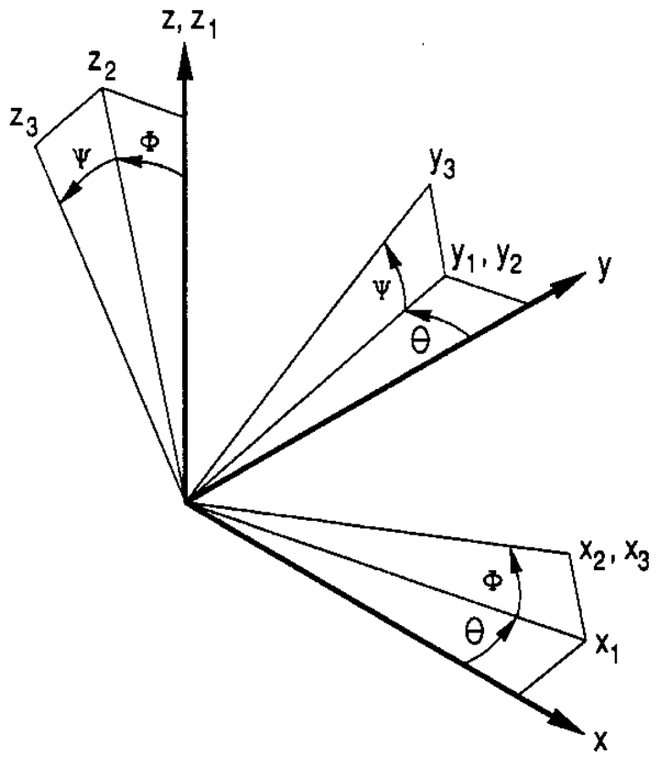

Figure 10: Euler Angle Tranformation

For each of the rotations, a simple transformation matrix can be found, and carrying them out successively leads to: $\mathbf{C}_v = \mathbf{C}_\psi\ \mathbf{C}_\phi\ \mathbf{C}_\theta$. Each of the Euler rotations gives a distinct component of the rotation vector, and they are related to the intermediate unit vectors as follows:

$$\omega_1 = \frac{\partial \psi}{\partial t}\mathbf{x}_2$$

$$\omega_2 = \mathbf{C}_\psi \frac{\partial \phi}{\partial t}\mathbf{y}_1$$

$$\omega_3 = \mathbf{C}_\psi \mathbf{C}_\phi \frac{\partial \theta}{\partial t}\mathbf{z}_w$$

In fact, vectorially, $\omega = \omega_1 + \omega_2 + \omega_3$, and this is sufficient knowledege to break up the rotation vector

into its three components in the vehicle frame $<\omega_{x_3},\omega_{y_3},\omega_{z_3}>$. Next, substitution is used to isolate the Euler Angle time rates of change, in terms of the angles themselves and these rotation vector components. Working through it, we obtain a result for **S**:

$$\mathbf{S} = \begin{bmatrix} 0 & \frac{\sin(\psi)}{\cos(\phi)} & \frac{\cos(\psi)}{\cos(\phi)} \\ 0 & \cos(\psi) & -\sin(\psi) \\ 1 & \frac{\sin(\phi)\sin(\psi)}{\cos(\phi)} & \frac{\sin(\phi)\cos(\psi)}{\cos(\phi)} \end{bmatrix}$$

14 ACKNOWLEDEGMENTS

The authors wish to acknowledge support from the MIT Sea Grant College Program under project number NA86AA-D-SG089; also support from the National Science Foundation, under subcontract from Woods Hole Oceanographic Institution, number SC-16670.